Multiharmonic Spanning Nonlinear X-wave: An Asymptotic State of Extreme Long Wave Infrared Dispersive Shock Regularization

Michael G. Hastings,* Paris Panagiotopoulos, Miroslav Kolesik, and Jerome V. Moloney
James C. Wyant College of Optical Sciences, University of Arizona, Tucson, Arizona 85721, USA
and Arizona Center of Mathematical Sciences, University of Arizona, Tucson, Arizona 85721, USA

(Received 21 December 2023; accepted 13 May 2024; published 18 June 2024)

We predict the emergence of novel X-waves emitted as a consequence of extreme dispersive shock regularization of an intense long wave few cycle pulse propagating through a weakly dispersive medium. This robust propagation-invariant solution to Maxwell's equations appears as the asymptotic state in the high harmonic conversion when the pump propagates in a strongly nonlinear weakly dispersive regime, while the weakly nonlinear conical emission is dominated by chromatic dispersion.

DOI: 10.1103/PhysRevLett.132.253801

In extreme nonlinear optics, broadband regions of anomalous and/or normal dispersion play a critical role in achieving strong spatiotemporal modification of ultrashort pulses in both condensed and gaseous bulk media where wavelengths range from the near infrared to long-wavelength infrared (LWIR) [1–5]. Near-IR filament propagation in such media is typically modeled by a generalized nonlinear Schrödinger equation (NLSE) [6] or its nonlinear envelope extensions [7,8]. Theberge [9] employing a multiterawatt near-IR 805 nm, 42 fs pulse, containing about 140 times the critical power for self-focusing, demonstrated a rather featureless ultrabroadband conical emission likely seeded from a many tens of randomly generated filaments. At longer wavelengths, however, the NLSE and its generalizations fail to accurately describe the relevant spatiotemporal reshaping of the pulse's underlying carrier field [10]. A new paradigm emerges as one transitions from a strongly dispersive, weakly nonlinear physical setting to a strongly nonlinear, weakly dispersive one as the driving laser wavelength tunes further into the transparency gap of the relevant material [10]. The canonical mathematical description of such ultrashort pulse evolution in this long-wavelength regime is given by a generalization of the well-known Kadomtsev-Petviashvili [11] equation (gKPE) which propagates the full, carrier-resolved field. Strong self-steepening of the optical carrier wave leads to shock formation [12] and, in the case of media with normal dispersion, singular gradients are regularized by the emission of a train of linear dispersive waves left in the wake of the main pulse.

In this Letter, we demonstrate that an intense, few cycle long wavelength driving pulse, can undergo extreme shocking and generate efficient conversion to high harmonics in weakly dispersive xenon gas. The end result, however, is not an emitted linear dispersive wave but instead a *nonlinear*, propagation-invariant X waveform. This asymptotic nonlinear X-wave spanning multiple harmonics, is remarkably robust maintaining its invariant waveform over more than a hundred Rayleigh ranges. The corresponding spectrum is a multi-octave spanning and very flat supercontinuum. The extreme bandwidth creates an interesting situation in which different parts of the total waveform require different mathematical descriptions, namely, gKPE for the pump pulse and NLSE for the nonlinear conical emission.

An X-wave or conical wave in nonlinear optics is a special case of space-time X-shaped wave packet [13] that is nearly propagation invariant both linearly and nonlinearly. Nonlinear X shapes may also appear in the angularly resolved spectra [14,15]. An X-wave as a non-spreading beam is generally formed from Bessel beams and holds together in the absence of nonlinearity. Pulsed X-wave packets can be thought of as a polychromatic superposition of Bessel beams [16]. A key feature of an X-wave pulse is that all spectral components travel with the same group velocity [17,18]. While these pulsed beams are not completely diffraction-free, the main peak of the transverse profile is well confined upon propagation.

In most physical settings it proves sufficient to employ either NLSE or gKPE in the spectral window of interest. For example, a recent work [19] confirmed that supercritical collapse singularities leading to attosecond duration subpulses in an anomalously dispersive medium can be adequately captured by a gKPE model using only the local dispersion within the transparency window around the driving pulse 10 μm wavelength. Here we identify a truly novel scenario where the cascade of nonlinear interactions transcends such local descriptions and propagation requires a full rigorous description ranging from the original pump driver wavelength at 10 μm all the way down to the deep UV. The physics over such a huge spectral span can only be captured by a Maxwell-level gUPPE propagator model [20]. The radially symmetric gUPPEcore [20,21] used here includes all relevant

physical processes such as diffraction, the Kerr effect [22], and tunnel ionization [23].

Among the inert gases, xenon proves to be an ideal test bed as it has one of the stronger Kerr nonlinearities and an extremely flat weakly normal dispersion that monotonically grows towards the UV with no intervening resonances [24]. When an intense, long-wavelength pulse is launched into a xenon cell, it initially experiences a weakly dispersive, strongly nonlinear propagation regime governed by gKPE. Shocks forming on the carrier are not regularized via the emission of weakly dispersive *linear* radiation from the rear of the pulse but instead the asymptotic state following extreme shocking is a robust *nonlinear* waveform that spans multiple octaves in frequency and maintains its shape over more than a hundred Rayleigh ranges. In contrast to the pump pulse described by the gKPE paradigm, the propagation of the emitted waveform is dominated by the chromatic dispersion in an NLSE-type weakly nonlinear regime. The carrier-wave shocking that starts the emission process is illustrated in Fig. 1 for an initially collimated 10 μm Gaussian pulse (black dotted curve) with a duration of 34 fs at full width half maximum (FWHM), a beam waist of 2.83 mm (at $1/e^2$ radius), a peak intensity of 5×10^{16} W/m^2, and initial energy of 27 mJ.

Shock development is a function of local field amplitude, thus we expect carrier wave steepening to develop in the central, most intense part of the electric field first. In Fig. 1(a) we can see that self-steepening is reshaping the carrier wave into a shark-fin form after just 10 cm of propagation, with much stronger distortions obvious at 60 cm [Fig. 1(b)]. After 80 cm of propagation, the first sign of dispersive regularization becomes evident [Fig. 1(c)] as a high-amplitude, high-frequency wave developing in the trailing part of the pulse. This dispersive wave is clearly beginning to separate from the main pulse past $z = 95$ cm [Fig. 1(d)], while at the same time surpassing the driving 10 μm field in amplitude. The high intensity of the emitted waveform implies that it propagates in a nonlinear regime, and the high frequency means that it experiences stronger (than the fundamental) chromatic dispersion. The peak intensity of the dispersive wave shed by the full driving pulse is sufficiently strong to generate a high density few micron thick narrow plasma channel with on-axis densities reaching 10^{23} m^{-3}. Since this waveform is sharply peaked on axis, there is some interaction with the free electrons which also concentrate in the same region. While the strong-field ionization does not destroy the self-healing conical wave [25], it does influence the nonlinear interactions in the on-axis region which in turn influences the resulting "group velocity of the material response wave." [17]. Notably, there is no indication of a self-focusing collapse for the long-wavelength waveform, as its peak amplitude remains fairly stable throughout.

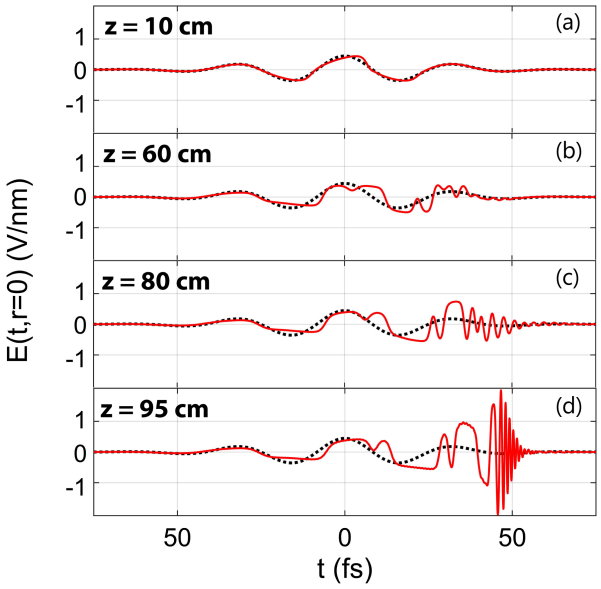

FIG. 1. On-axis electric field $E(t, r = 0)$ vs time for several propagation distances in xenon gas. Gray dotted curve represents the input electric field of the 34 fs, 10 μm Gaussian pulse. Red curves: electric fields at (a) $z = 10$, (b) $z = 60$, (c) $z = 80$, and (d) $z = 95$ cm.

Figure 2 illustrates the same dynamics in the so-called angle-resolved spectra, which show the spectral power density of the waveform as a function of the frequency and transverse wave number $k_\perp$ for several propagation distances, starting from the spectrum of the initial pulse in Fig. 2(a). While the shocks develop almost instantaneously (cf. Fig. 1), the spectral emission remains near on axis, i.e., concentrated around $k_\perp = 0$, in $(k_\perp, \omega)$ up to $z = 80$ cm [Figs. 2(b) and 2(c)] due to the very small GVD of xenon. Subsequently, across the relatively short distance from $z = 80$ to $z = 95$ cm [Figs. 2(c)–2(e)], we observe the rapid evolution to a pronounced conical-wave feature depicted in Fig. 2(f). What sets this structure apart from the conical emission generated by near-infrared pulses [15,17,18] is the extraordinary wide spectrum which extends beyond the 25th harmonic frequency of the pump pulse.

The conical emission in Fig. 2(f) can be described by the so-called X-wave dispersion relation, which identifies conical beams traveling with the same group velocity [17,26];

$$k_\perp(\omega) = \sqrt{\left(\frac{\omega n(\omega)}{c}\right)^2 - \left(\frac{\omega_0 n(\omega_0)}{c} + \frac{\omega - \omega_0}{v_g}\right)^2}, \qquad (1)$$

where ω_0 and v_g are the central on-axis frequency and the group velocity of the waveform, respectively. The latter usually matches the speed of the nonlinear perturbation in the medium [17], and can be different from the group velocity corresponding to the central frequency. The black line superimposed on the conical-wave feature in Fig. 2(f) corresponds to $\omega_0 = 1.6952 \times 10^{15}$ rad/s and $v_g = 299{,}591{,}210$ m/s. The effective group velocity reflects

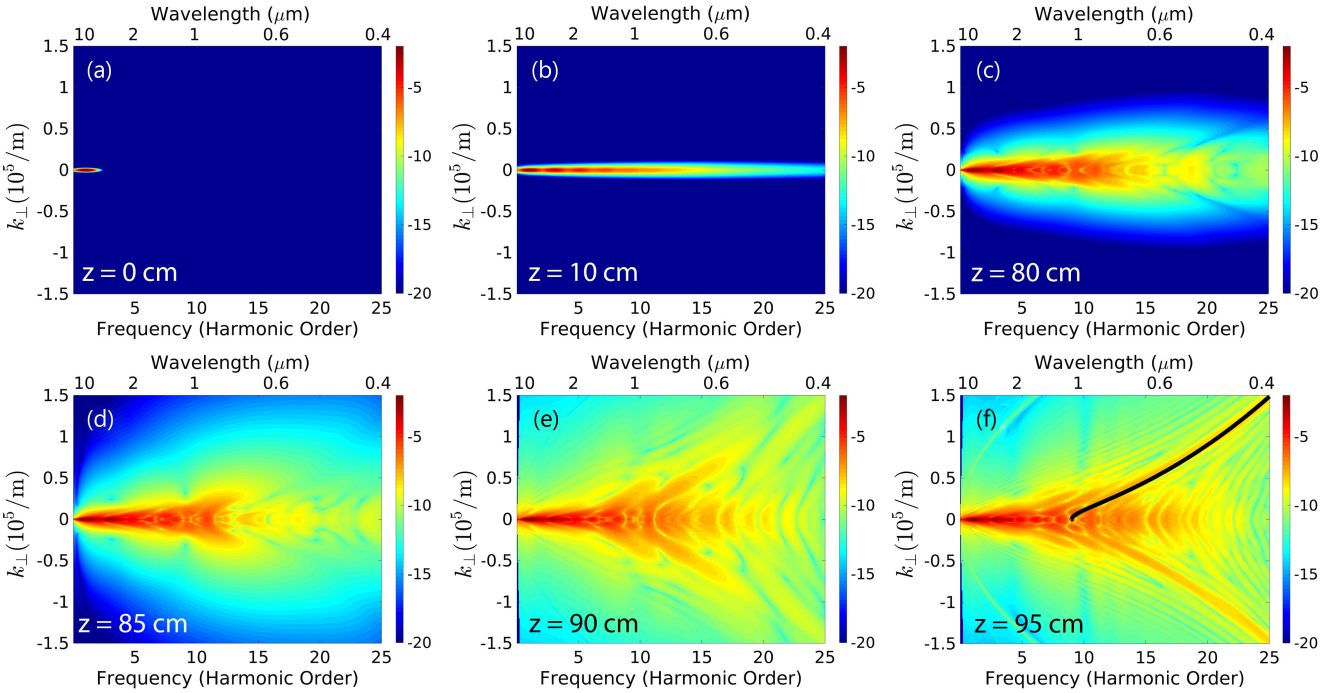

FIG. 2. Angle-resolved spectrum $(k_\perp, \omega)$ at various propagation distances in xenon. (a) Input pulse, (b) initial supercontinuum generation at $z = 10$ cm, (c)–(e) formation of conical emission $z = 80$–90 cm, (f) fully formed X-wave $z = 95$ cm. The black line overlaid on the X-wave arm (f) corresponds to the X-wave dispersion relation (1) with $v_g = 299, 591, 210$ m/s.

a complex dynamics which includes freed electron generation and subsequent plasma-induced defocusing. This observation suggests that the extended structure, hereafter called the X-wave arm, seen in the angle-resolved spectrum corresponds to an X-wave. However, to the best of our knowledge, X-waves were never observed or even simulated with such an extreme bandwidth. This is why we proceed with further tests to probe the properties of this unusual waveform.

In order to verify that the feature in Fig. 2(f) is indeed a multi-octave X-wave, one needs to isolate its waveform from the rest of the pulse, and demonstrate that (i) in real space (r, t) the wave packet exhibits a localized central peak together with a characteristic X-shape, (ii) it propagates with little diffraction and/or dispersion, both in the linear (Kerr-effect off) and nonlinear regimes (i.e., with the full medium response included).

Using the X-wave dispersion relation (1) as a guide, we can apply a spectral filter in $(k_\perp, \omega)$ space to select only the plane waves with frequencies and transverse wave numbers in a close vicinity of the locus given by (1). This way we isolate the relevant spectral content from the rest of the light, i.e., from both the other weaker conical emissions evident in the angle-resolved spectrum and from the spectrally broadened driving pulse. The effect of the filter is depicted in Figs. 3(a) and 3(b), showing the full and the filtered spectrum, respectively. The spectrum shown in Fig. 3(a) is a reproduction of Fig. 2(f) with expanded x and y axes as well as a different color bar to highlight the

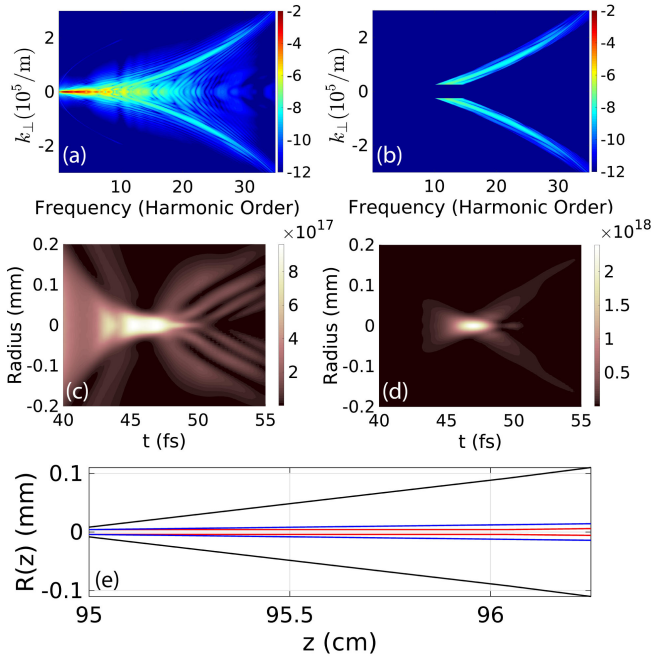

FIG. 3. Far-field spectrum $(k_\perp, \omega)$ at $z = 95$ cm, of the full wave packet (a), and filtered multi-octave conical wave (b). (c) and (d) Corresponding spatiotemporal intensity distributions $I(r, t)$. (e) Beam waist evolution over 10 Rayleigh lengths of the multiharmonic X-wave in the linear (blue curve) and nonlinear (red curve) xenon. Black curve: Linear Gaussian beam of the same starting waist of 20 μm. The energy contained in the filtered X-wave is 77 μJ.

strongest features in the X-wave arm and suppress low amplitude spectral background.

Transforming the full and the filtered spectral amplitudes back into real space of (r, t), one obtains their respective spatiotemporal waveforms, and their intensities shown in panels (c) and (d) of Fig. 3. The important feature in panel (d) is the subtle X-shape emanating from the central peak. Here it serves as further evidence that the emissions from the shock forming in the carrier-wave at 10 μm are spontaneously "orchestrated" into a well-localized, broad-bandwidth wave packet. The energy contained in the filtered pulse [Fig. 3(d)] is 77 μJ, corresponding to a conversion efficiency of 0.285%. While the conversion efficiency may seem low, it should be noted that this energy is only for one of a number of emitted X-waves and represents only the X-wave arm, so no contribution from $(k_\perp = 0, \omega)$.

Having isolated the relevant waveform from the rest of the pulse, we can test its propagation and compare it to that of an equivalently sized Gaussian beam (≈20 μm at $1/e^2$ radius). We proceed to simulate the propagation for 100 Rayleigh ranges, from $z = 95$ to $z = 107.5$ cm, in xenon in both linear (realized by switching off the Kerr effect) and nonlinear regimes (i.e., with the full medium response) to verify that the diffraction is very weak as is expected for an X-wave. The red and blue curves in Fig. 3(e) depict the beam sizes (FWHM) of the filtered X-wave vs propagation distance over 10 Rayleigh lengths, in normal xenon (nonlinear) and xenon with n_2 set to zero (linear propagation), respectively. We can clearly see that the wave packet is experiencing only minor beam spreading over the 10 Rayleigh ranges of propagation shown, in both linear and nonlinear settings. It stays confined over about more than 100 Rayleigh ranges (data not shown), while the nonlinear waveform is held even more tightly localized by the nonlinearity. For comparison, the equivalent linear Gaussian beam (black curve) is showing a much faster beam spreading.

The above analysis confirms that the conical feature highlighted in Fig. 2(f) and the corresponding spatiotemporal waveform with the intensity profile shown in Fig. 3(d) is indeed an X-wave with an extreme bandwidth spanning from roughly 1.1 μm to over 35 harmonic orders of the fundamental frequency that was used to generate it. Such prominent X-wave features could be interpreted as signatures of field shocking in high field LWIR sources [27].

We can further study the physics that led to the generation of this multi-octave X-wave by isolating its on-axis spectral content by selectively time gating it as depicted in Fig. 4(a), where the two red vertical lines mark the extent of the temporal gate. After Fourier transforming the time-gated electric field between the red lines, we obtain the on-axis spectrum shown in the red curve in Fig. 4(b), which is superimposed to the full on-axis spectrum of the full pulse [black curve in Fig. 4(b)]. It is evident that the on-axis wave contains the majority of the generated supercontinuum beyond the 9th harmonic. This is no coincidence, as the arms of the X-wave in the $(k_\perp, \omega)$

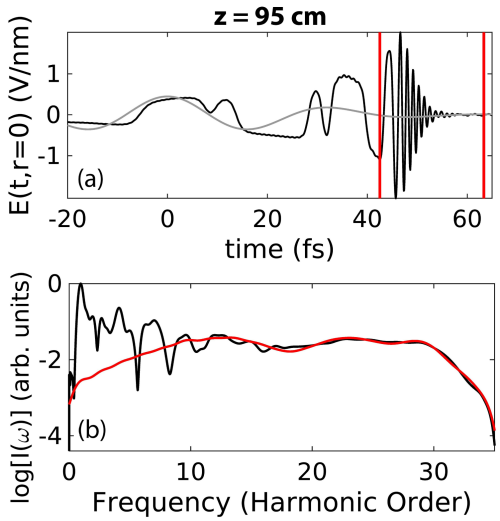

FIG. 4. Time-gating of the dispersive wave. (a) On-axis electric field $E(t, r = 0)$, of the initially 34 fs pulse in xenon at (gray) $z = 0$ and (black) at $z = 95$ cm. (b) (red) Spectral intensity of corresponding to the temporal profile between the two red vertical lines in (a). (Black) Spectral intensity of the entire on-axis electric field. The entire supercontinuum from the 10th harmonic to the 30th harmonic contains 145 μJ of energy.

spectrum have their on-axis origin in this frequency region. The flatness of the spectrum indicates a highly coherent single-pulse waveform.

In order to better understand the role of the driving-pulse wavelength, we have conducted additional simulations (results not shown here) in which we varied the wavelength between 5 to 10 μm while maintaining the same input pulse intensity, ensuring that different pulses experienced similar initial carrier-wave self-steepening. We found that the multi-octave X-wave always develops, albeit with a slight shift in its central wavelength. Nonetheless, its central λ always falls between 1 and 1.5 μm. This qualitative transition between the strong-nonlinearity and weak-dispersion regime (gKPE) and strong-dispersive and weakly nonlinear NLSE regime is best understood by comparing the relative group velocity dispersion of the fundamental and strongest growing harmonic (third) at the 10 μm driving wavelength which are close due to the flat dispersion. Reference [28] introduces a carrier shock dispersive length scale as proportional to the inverse difference of this quantity. When this length exceeds the nonlinear length scale, depending inversely on field intensity, we expect formation of shocks. Because of the extremely broad and flat supercontinuum, the X-wave frequency is now automatically selected where the regime crossover from gKPE to NLSE is taking place. Following the formulation in [10,28], we find that this transition in xenon happens roughly between 1–1.3 μm, which corresponds to the 9th harmonic of our 10 μm main study case. In simple words, the mechanism can be traced back to the fact that the driving pulse generates broadband higher

harmonic content, which in this case (due to the xenon dispersive landscape) can become intense enough that it itself can produce it own self-steepening and carrier wave shock formation, which in turn leads to the generation of a large family of conical waves, all contained in the intense waveform trailing the pump pulse. Because of the extreme broadband nature of the whole wave packet, and the fact that there is continuous conversion from the fundamental effectively replenishing the energy in the X-wave, these X-waves are now much more intense and extremely broadband compared to traditional X-waves, which are typically only found around the fundamental or a seed wavelength.

We remark finally that there are ongoing efforts worldwide to push LWIR single or few cycle sources towards the energies quoted here. These range from OPCPA generated 2 mJ 7 μm pulses being extended to 20 mJ [29] or an alternative path to 100 fs or so, 100 mJ pulses starting from variants of optically pumped high energy CO_2 lasers [30]. A recent novel experiment demonstrated 3–4 mJ single cycle LWIR pulses by exploiting photon deceleration in plasma wakes by Nie *et al.* [31].

In summary, we predict a novel extreme nonlinear phenomenon whereby a long wave few cycle intense pulse in weakly dispersive xenon gas can develop extreme gradients (shocks) greatly distorting the underlying optical carrier wave, and emit a strong near-IR multiharmonic spanning X-wave with a peak amplitude that can approach that of the pump pulse. The formation of an X-wave in the near-IR is robust regarding initial pulse wavelength in the mid-IR and marks the crossover frequency from a nonlinear dominated (gKPE description) to dispersion dominated (NLSE description) regime. We predict that this phenomenon should be common across other inert gases, and transparent media with similar dispersive properties.

This material is based upon work supported by an Air Force Office of Scientific Research (AFOSR) Grant No. FA9550-21-1-0463.

*mghastings@arizona.edu

[1] M. Durand, A. Jarnac, A. Houard, Y. Liu, S. Grabielle, N. Forget, A. Durécu, A. Couairon, and A. Mysyrowicz, Phys. Rev. Lett. **110**, 115003 (2013).
[2] A. A. Voronin and A. M. Zheltikov, Phys. Rev. A **95**, 023826 (2017).
[3] A. A. Voronin and A. M. Zheltikov, Opt. Lett. **42**, 3614 (2017).
[4] D. Kartashov, S. Ališauskas, A. Pugžlys, A. Voronin, A. Zheltikov, M. Petrarca, P. Béjot, J. Kasparian, J.-P. Wolf, and A. Baltuška, Opt. Lett. **38**, 3194 (2013).
[5] V. Shumakova, S. Ališauskas, P. Malevich, A. A. Voronin, A. V. Mitrofanov, D. A. Sidorov-Biryukov, A. M. Zheltikov, D. Kartashov, A. Baltuška, and A. Pugžlys, Opt. Lett. **44**, 2173 (2019).
[6] J.-C. Diels and W. Rudolph, *Ultrashort Laser Pulse Phenomena Fundamentals, Techniques, and Applications on a Femtosecond Time Scale Second Edition* (Academic Press, New York, 1996).
[7] T. Brabec and F. Krausz, Phys. Rev. Lett. **78**, 3282 (1997).
[8] A. Couairon and A. Mysyrowicz, Phys. Rep. **441**, 47 (2007).
[9] F. Théberge, M. Châteauneuf, V. Ross, P. Mathieu, and J. Dubois, Opt. Lett. **33**, 2515 (2008).
[10] P. Whalen, P. Panagiotopoulos, M. Kolesik, and J. V. Moloney, Phys. Rev. A **89**, 023850 (2014).
[11] B. Kadomstev and V. Petviashvilli, Sov. Phys. Dokl. **15**, 539 (1970).
[12] P. Kinsler, J. Opt. Soc. Am. B **32**, 1889 (2015).
[13] E. Recami, Physica (Amsterdam) **252A**, 586 (1998).
[14] P. Di Trapani, G. Valiulis, A. Piskarskas, O. Jedrkiewicz, J. Trull, C. Conti, and S. Trillo, Phys. Rev. Lett. **91**, 093904 (2003).
[15] M. Kolesik, E. M. Wright, and J. V. Moloney, Phys. Rev. Lett. **92**, 253901 (2004).
[16] J. Salo, J. Fagerholm, A. T. Friberg, and M. M. Salomaa, Phys. Rev. E **62**, 4261 (2000).
[17] M. Kolesik, E. M. Wright, and J. V. Moloney, Opt. Express **13**, 10729 (2005).
[18] A. Couairon, D. Faccio, and P. Di Trapani, *Conical Waves, Filaments and Nonlinear Filamentation Optics*, Area 02: Physical Science (Aracne, Rome, 2007).
[19] A. Hofstrand and J. V. Moloney, Phys. Rev. Lett. **124**, 043901 (2020).
[20] M. Kolesik and J. V. Moloney, Phys. Rev. E **70**, 036604 (2004).
[21] P. Panagiotopoulos, P. Whalen, M. Kolesik, and J. V. Moloney, Nat. Photonics **9**, 543 (2015).
[22] M. Tarazkar, D. A. Romanov, and R. J. Levis, Phys. Rev. A **90**, 062514 (2014).
[23] T. D. G. Walsh, J. E. Decker, and S. L. Chin, J. Phys. B **26**, L85 (1993).
[24] A. Bideau-Mehu, Y. Guern, R. Abjean, and A. Johannin-Gilles, J. Quant. Spectrosc. Radiat. Transfer **25**, 395 (1981).
[25] M. Kolesik and J. V. Moloney, Opt. Lett. **29**, 590 (2004).
[26] D. Faccio, A. Averchi, A. Lotti, P. D. Trapani, A. Couairon, D. Papazoglou, and S. Tzortzakis, Opt. Express **16**, 1565 (2008).
[27] P. Kinsler, S. B. P. Radnor, J. C. A. Tyrrell, and G. H. C. New, Phys. Rev. E **75**, 066603 (2007).
[28] P. Panagiotopoulos, P. Whalen, M. Kolesik, and J. V. Moloney, J. Opt. Soc. Am. B **32**, 1718 (2015).
[29] Jens Biegert, Institute of Photonic Sciences in Barcelona (private communication).
[30] Yu-Hsin Chen, Daniel F. Gordon, Victor Hasson, Soumya Sarang, and Martin Richardson, in High Power Laser Ablation Conference, *High-Power Ultrashort Lasers for Materials Science and Particle Acceleration* (SPIE, Santa Fe, NM, 2024); private communication.
[31] Z. Nie, C.-H. Pai, J. Zhang, X. Ning, J. Hua, Y. He, Y. Wu, Q. Su, S. Liu, Y. Ma, Z. Cheng, W. Lu, H.-H. Chu, J. Wang, C. Zhang, W. B. Mori, and C. Joshi, Nat. Commun. **11**, 2787 (2020).